

PACS numbers: 07.85.Fv; 42.55.Vc
DOI: 10.1070/QE2012v042n02ABEH014770

Aperiodic multilayer structures in soft X-ray radiation optics

E.A. Vishnyakov, F.F. Kamenets, V.V. Kondratenko, M.S. Luginin, A.V. Panchenko, Yu.P. Pershin, A.S. Pirozhkov, E.N. Ragozin

Abstract. **We review the works related to the development of aperiodic multilayer structures – optical elements for the soft X-ray range. The potentialities of aperiodic multilayer mirrors as regards reflection of soft X-ray radiation in a broad wavelength range, first and foremost at normal radiation incidence, as well as the capabilities of broadband polariser mirrors are investigated. The results of multiparametric optimisation and experimental results for Mo/Si aperiodic mirrors ($\lambda \geqslant 12.5$ nm) as well as calculations for several promising material pairs (Pd/Y, Ag/Y, etc.) for $\lambda \leqslant 12.5$ nm are outlined. The effect of transition layers on the reflectivity is considered, in particular by taking into account the smooth variation of the permittivity near interfacial boundaries. The use of broadband mirrors in laser-plasma spectroscopic experiments is discussed.**

Keywords: *soft X-ray range, broadband multilayer mirrors, transition layers, aperiodic multilayer structures.*

1. Introduction

More than 30 years have passed since the first suggestion and implementation of the idea of an X-ray multilayer mirror and its consistent theoretical analysis [1, 2]. This period has seen the development of the methods of synthesis, characterisation, and calculation of the multilayer optics in a broad wavelength range in the vacuum ultraviolet (VUV) and X-ray spectral domains (~50–0.02 nm), which corresponds approximately to the photon energy range between 25 eV and 60 keV. In this case, the emphasis was primarily made on periodic multilayer structures capable of affording – for a fixed angle of radiation incidence – a rather high reflection coefficient in a relatively narrow wavelength interval. The reflection coefficient of a periodic structure is at its maximum at a wavelength $\lambda_0 \approx 2d\langle n\rangle\cos\theta/m$, where d is the structure period (i.e. the sum of the layer thicknesses of materials A and B, which alternate in the structure); $\langle n\rangle$ is the value of refractive index averaged over the structure period; θ is the angle of incidence; and m is the order of reflection. [Note that we are dealing with a binary structure $\{A/B\}_N$; more complex structures, for instance ternary structures, are also considered in certain special cases. At this point we omit transition layers with a mixed elemental composition, which inevitably make their appearance at the interfaces, nor we discuss barrier layers purposefully deposited in special cases to prevent the formation of excessively thick transition layers (see below).]

Multilayer mirrors (MMs) based on periodic structures enjoy wide use in the spectroscopy of laboratory plasmas, X-ray astronomy, analytical instrument making, and the optics of laboratory VUV and X-ray radiation sources, including synchrotrons and free-electron lasers.

Along with periodic multilayer structures, also of interest are aperiodic structures which are capable of satisfying other criteria than the attainment of a high reflection coefficient in a relatively narrow wavelength interval. In the class of aperiodic multilayer structures (MSs) it is possible to solve a number of optimisation problems which are of practical significance in X-ray optics, including the optics of the soft X-ray (SXR) range [3]. Among these problems are, for instance, calculation and fabrication of MSs which provide: (i) the highest possible uniform reflectivity throughout a given interval of wavelengths or angles of incidence; (ii) a high polarisance over a broad wavelength range for a fixed angle of radiation incidence; (iii) the highest possible reflection coefficient at one or several wavelengths; (iv) the highest possible integral reflectivity of a single mirror or the highest possible integral transmission coefficient for a system consisting of several sequentially arranged MMs, filters, etc. The inclusion of the phase of amplitude reflection coefficient (along with its modulus) permits determining the structures suitable for reflecting attosecond SXR pulses and manipulating their shape and duration [4, 5].

The idea of making a broadband multilayer mirror and treating the thicknesses of individual layers of the structure as independent variables (optimisation parameters) in the solution of a multiparametric optimisation problem was conceived, presumably for the first time, in the solution of X-ray astronomy problems [6]. The authors of Ref. [6] set themselves the task to calculate the structures possessing the maximum integral reflection coefficient

$$\Im_\lambda = \int_{\lambda_1}^{\lambda_2} R(\lambda)\mathrm{d}\lambda$$

in the wavelength ranges 30–60 nm (an Ir/Si structure) and 10–30 nm (Pt/Si) at near-normal radiation incidence. More

E.A. Vishnyakov, M.S. Luginin, E.N. Ragozin P.N. Lebedev Physics Institute, Russian Academy of Sciences, Leninsky prosp. 53, 119991 Moscow, Russia; Moscow Institute of Physics and Technology (State University), Institutskii per. 9, 141700 Dolgoprudnyi, Moscow region, Russia; e-mail: juk301@mail.ru, enragozin@gmail.com;
F.F. Kamenets, A.V. Panchenko Moscow Institute of Physics and Technology (State University), Institutskii per. 9, 141700 Dolgoprudnyi, Moscow region, Russia;
V.V. Kondratenko, Yu.P. Pershin National Technical University 'Kharkov Polytechnic Institute', ul. Frunze 21, 61002 Kharkov, Ukraine;
A.S. Pirozhkov Advanced Beam Technology Division, JAEA, 8-1-7 Umemidai, Kizugawa, Kyoto, 619-0215, Japan

Received 17 November 2011
Kvantovaya Elektronika **42** (2) 143–152 (2012)
Translated by E.N. Ragozin

recently, endeavours were undertaken to calculate and synthesise Mo/Si-based structures possessing either the maximum integral reflectivity or the maximum uniform reflectivity in a given wavelength interval [7]. Specifically, a structure was found, which provided a uniform reflectivity $R \sim 30\%$ in the 15–17 nm range at normal radiation incidence. The problem of a MM capable of reflecting soft X-ray radiation at two wavelengths was also considered [8].

One cannot help mentioning the works dedicated to the development of MSs for a harder X-ray range. The feasibility of applying grazing-incidence multilayer optics in a Kirkpatrick–Baez telescope for hard X-rays was analysed in Ref. [9]. The authors reported the synthesis of a W/Si MM intended for the reflection of X-ray radiation with photon energies up to 69 keV (0.18 Å) at a grazing incidence angle of 3 mrad. The MM period decreased monotonically with depth in the structure (the concept of a so-called supermirror). An analytical method and later a numerical algorithm [10] were proposed for calculating aperiodic mirrors with a given reflectivity profile in the hard X-ray range. The works in this direction have found use, in particular, in synchrotron radiation optics [11].

Here our concern is primarily with the wavelength interval 3–30 nm, which belongs to the soft X-ray range of the vacuum UV domain of the spectrum. As is commonly known, in this range it is possible to make rather efficient normal-incidence periodic MMs. The multilayer structures that possess a high reflectivity at normal incidence are particularly valued, because focusing normal-incidence multilayer optics is capable of imaging in the SXR range, including dispersive spectral imaging. 'Ordinary' periodic MSs offer a relatively narrow ($\Delta\lambda_{1/2}/\lambda \approx 0.01-0.1$) resonance spectral reflectivity profile, which makes them efficient instruments for constructing mostly quasimonochromatic spectral images. However, there is also a demand for normal-incidence MMs capable of reflecting radiation in a broad spectral wavelength range without changing the angle of radiation incidence. In particular, there is a demand for stigmatic optical and spectral instruments with a broad spectral operating band (of the order of an octave in wavelength, i.e. $\Delta\lambda/\lambda \sim 1/2$). This is possible with the employment of broadband (aperiodic) normal-incidence MMs in combination with diffraction gratings*, for instance, with a transmission grating (Fig. 1). Such an imaging diffraction spectrometer possesses simultaneously a broad spectral operating range, stigmatism, a large acceptance angle (~0.05 sr), and a high throughput for a spectral resolving power $\lambda/\delta\lambda \approx 200-1000$, i.e. the combination of properties previously inherent in spectrometers of only the visible, UV, and partly VUV ($\lambda \geqslant 50$ nm) regions.

The areas of application of broadband aperiodic mirrors and their based instruments comprise: the investigation of elementary processes with participation of multiply charged ions carried out with the use of stigmatic imaging spectrographs [12–20]; the diagnostics of plasmas, including laser-driven microplasmas; recording of the high-order harmonic spectra of laser radiation; recording of the SXR radiation pulses generated by free-electron lasers [21] or other sources; reflection of attosecond SXR pulses and their duration conversion [4, 5], etc. The task of maximising the integral transmission coefficient for several sequential reflections in a system of mirrors with the inclusion of filter transmittance

*Construction of dispersed spectral images is also possible with multilayer reflection diffraction gratings. The case in point is a concave diffraction gratings with a multilayer structure deposited on top of it.

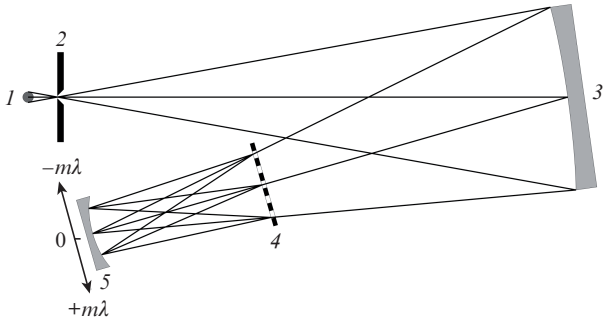

Figure 1. Schematic diagram of an imaging (stigmatic) spectrometer: (*1*) source (laser plasma); (*2*) input spectrometer slit; (*3*) multilayer mirror mounted at near-normal radiation incidence; (*4*) free-standing transmission grating; (*5*) focal surface.

emerges, in particular, in X-ray lithography. Recently, a Mo/Si MM optimised for maximum uniform reflectivity in the 12.5–25 nm range for normal radiation incidence was employed in experiments involving the conversion of Ti:sapphire laser radiation ($\lambda \sim 0.8$ μm) to SXR radiation. The frequency upconversion took place in the reflection from the relativistic plasma wave generated by a multiterawatt laser in a pulsed helium jet (a relativistic 'flying mirror') [22–24]. Optical schemes which rely only on normal-incidence mirrors are higher in value than grazing-incidence schemes, since they exhibit substantially lower aberrations and are therefore suited for the formation of optical images – provided, of course, it is possible to make the requisite aperiodic structures with sufficiently high reflection efficiency.

For our first step we employed a molybdenum-silicon MS, which exhibits high reflectivity in the range $\lambda > 12.5$ nm. Subsequently we plan to extend our approach to the domain below the L absorption edge of silicon ($\lambda < 12.5$ nm), which necessitates the use of other material pairs.

2. Calculation of aperiodic multilayer mirrors. Inclusion of transition layers

The numerical technique described in this Section enables optimising a multilayer structure for various criteria. Its efficiency has been demonstrated in the optimisation of aperiodic MSs intended for operation in any subrange of the X-ray spectral range for different angles (including small grazing angles) of radiation incidence, even though the number of structure layers may be quite large (~10^3). The principal goal (but not the sole one) of our calculations was the quest for aperiodic MSs with as broad as possible a uniform reflection band.

Consider a multilayer structure $\{l_j\}, j = 1, \ldots, N$, consisting of N alternating layers characterised by complex permittivities of the form $\varepsilon_{A,B} = n_{A,B}^2 = 1 - \delta_{A,B} + i\beta_{A,B}$. For materials consisting of atoms of one sort, the optical constants $\delta_{A,B}$ and $\beta_{A,B}$ are related to atomic scattering factors $f = f_1 + if_2$ by the formula

$$\begin{pmatrix}\delta\\ \beta\end{pmatrix} = \frac{r_0}{\pi}\lambda^2 N\begin{pmatrix}f_1\\ f_2\end{pmatrix} \approx 0.54\times 10^{-5}\frac{\rho}{\mu}\lambda_a^2\begin{pmatrix}f_1\\ f_2\end{pmatrix},$$

where $r_0 = e^2/(m_e c^2) \approx 2.8. \times 10^{-13}$ cm is the classical electron radius; N is the atomic number density; μ is the atomic mass; λ_a is expressed in Angstroms and the material density ρ in grams per cubic centimetre. When the material comprises

atoms of several sorts, there applies a more general expression:

$$\begin{pmatrix}\delta\\ \beta\end{pmatrix} \approx 0.54\times 10^{-5}\frac{\rho}{\sum_i \alpha_{1i}\mu_i}\lambda_a^2\begin{pmatrix}\sum_i \alpha_{1i} f_{1i}\\ \sum_i \alpha_{1i} f_{2i}\end{pmatrix},$$

where α_i is the fraction of the atoms of sort i. The data about atomic scattering factors for elements with atomic numbers from 1 to 92 in the 10 eV–30 keV photon energy range are available from the literature [25].

The layer thicknesses l_j are, generally speaking, different. Unlike a periodic structure, the sum thicknesses of adjacent layer pairs are not assumed to be constant with depth in the structure: $l_1 + l_2 \neq l_3 + l_4 \neq \ldots$. The optical path lengths for neighbouring layer pairs are, generally speaking, not equal, either: $l_1 n_A + l_2 n_B \neq l_3 n_A + l_4 n_B \neq \ldots$. Furthermore, the existence of a structure period in any sense is not *a priori* assumed.

The structure reflection coefficient $R_{s,p}(\lambda, \theta)$ for s- and p-polarised radiation incident at an angle θ (the direct problem of multilayer optics) was calculated by the method of recurrent relations described in the literature [26, 27] and repeatedly used by several authors. The problem of finding the aperiodic MS which best satisfies some preassigned criterion will be referred to as the inverse problem of multilayer optics or the aperiodic MS (AMS) optimisation problem. A goal function F_{gf} was specified for $R_{s,p}(\lambda, \theta_0)$ or $R_{s,p}(\lambda_0, \theta)$ (the subscript '0' signifies that the angle of incidence or the wavelength are fixed). The goal function may be specified on some interval of wavelengths or angles of incidence as well as on several isolated intervals. We introduce the norm of departure of the reflection coefficient from F_{gf} (the merit function F), which is calculated in the definition domain of F_{gf} and treated as a function of N variables $\{l_j\}$. Then, a numerical technique is employed to find the AMS by minimising the functional $F = \int[R(\lambda) - F_{gf}]^{2m} d\lambda$ $(m = 1, 2, \ldots)$. The functions F_{gf} and F are selected proceeding from the nature of the problem under solution and predetermine the optimisation result. In this case, the number of optimisation parameters is equal to the number of layers in the aperiodic structure. To find the extremum of the F functional, advantage was taken, in particular, of a genetic algorithm and the method of steepest descent. To decrease the power of the dependence of the computation time on N, an analytical formula was derived for the partial derivatives of the amplitude reflection coefficient with respect to layer thicknesses [3].

We concerned ourselves primarily with multilayer structures and mirrors suitable for operation as the focusing elements of a spectrometer with a broad spectral operating range. The aperiodic MSs of this kind were optimised to achieve the highest uniform reflectivity over the prescribed wavelength range by minimising the functional

$$F = \int_{\lambda_1}^{\lambda_2} [R(\lambda) - R_0]^{2m} d\lambda .$$

The computed aperiodic MSs possess, as a rule, a substantially higher integral reflection coefficient in comparison with any periodic mirror whose resonance reflection peak is located in the same wavelength interval. Periodic structures served as the initial structures in the solution of these optimisation problems. In this case, it turned out different initial structures may lead to practically equipollent (from the optimisation criterion standpoint) solutions, despite the fact that their corresponding (optimised) AMSs were substantially different in layer thickness sets l_j. At the same time, the question of finding the absolute (global) minimum of F remained an open question.

In the calculation of reflection characteristics of MMs, account should be taken of the possible imperfections of the fabricated MSs themselves. Among the variety of observed defects (the presence of impurities, departure of layer densities from the tabulated values, the state of the MS surface, etc.), of paramount importance in impairing the optical characteristics of an MS are its interphase roughness and transition layers. When individual layers are deposited by sputtering techniques (ion-beam, magnetron, triode sputtering, etc.), the substrate roughness is, as a rule, reproduced in the coating, and therefore today the availability of substrates with a roughness smaller than 2 Å permits regarding the roughness problem as being of minor importance. However, the existence of transition layers, which result from interdiffusion in the MS fabrication, has a consequence that the permittivity of pure materials A and B varies from ε_A to ε_B over the thickness of transition layer. The degree of mixing and the composition of transition layer depend on the technique and conditions of Mo/Si MS fabrication, and the thickness of transition layer may vary from 6–12 Å [28] to 30 Å [29] and its composition from $MoSi_2$ [30] to Mo_5Si_3 [31]. In our case, as the data of transverse-section electron microscopy suggest [12–20], in the Mo/Si structure the Mo-on-Si transition layer thickness is equal to about 12 Å and the Si-on-Mo transition layer thickness is equal to about 6 Å (Fig. 2) when the underlying Mo layer thickness is not less than ~20 Å, the elemental composition of transition layer being close to the silicide $MoSi_2$ [28].

The inclusion of transition layers in a periodic structure lowers the peak reflection coefficient by several percent. Specifically, in the Mo/Si periodic structure optimised for maximum reflectivity at λ = 13.5 nm in Mo-layer-to-period ratio, the inclusion of transition layers results in a lowering of the peak reflection coefficient from 74.6% to 71.6%. A more realistic description of the effect of transition layers on the

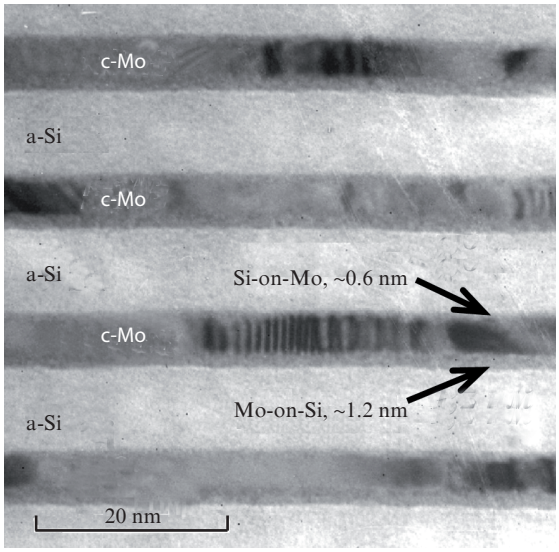

Figure 2. Electron microscope image of the transverse section of a periodic Mo/Si MS with a period of 153 Å, which shows the existence of transition layers between the layers of amorphous silicon (a-Si) and crystalline molybdenum (c-Mo).

structure reflectivity takes into account the smooth character of permittivity variation at the interface. This inclusion is mathematically achieved, for instance, by way of multistep approximation of the transition using a linear interpolation of ε. Figure 3a shows the reflectivity profile of a periodic MM (Mo/Si, $\lambda_0 = 13.5$ nm) with and without the inclusion of transition layers; shown in Fig. 3b is the behaviour of the peak reflectivity when the difference $\varepsilon_{Mo} - \varepsilon_{Si}$ is approximated by a variable number of steps as well as when the transition layer is approximated by a layer with the stoichiometry of silicide $MoSi_2$. One can see that the peak reflectivity slightly increases and tends to a constant value with increase in the number of steps. This limiting value is approximately 1% higher than the value obtained when the transition value is included in the form of the silicide $MoSi_2$.

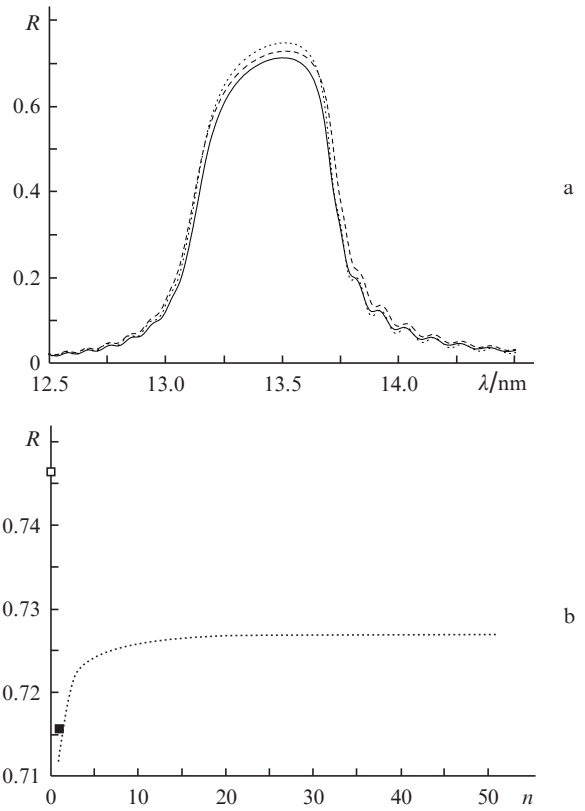

Figure 3. Calculated reflection coefficient of the Mo/Si periodic multilayer structure (150 layers) optimised for maximum reflection coefficient at $\lambda = 13.5$ nm without the inclusion of transition layers (the dotted curve), with the inclusion of one transition layer with $\varepsilon = (\varepsilon_{Mo} + \varepsilon_{Si})/2$ (solid curve) or a smooth transition of ε from ε_{Mo} to ε_{Si}, i.e. for $n \to \infty$ (dashed curve) (a). Calculated peak reflectivity without the inclusion of transition layers (□), with the inclusion of transition layers in the form of silicide $MoSi_2$ of thickness 6 Å (Si-on-Mo) and 12 Å (Mo-on-Si) (■), as well as approximation of the smooth transition of ε by a different number of intermediate steps n (b).

In the optimisation we introduced a programmable limit on the minimal layer thickness. This stems from the necessity to eliminate physically absurd solutions (a layer thickness may not be smaller than the dimension of an atom or a molecule) and improve the stability of the reflectivity of the MS being synthesised relative to the formation of transition layers (ideally, the thicknesses of 'pure' substance layers should far exceed the thicknesses of transition layers). An empirical rule was determined, whereby imposing the lower bound for a layer thickness at about a level of $\lambda_{min}/4$ (λ_{min} is the short-wavelength bound of optimisation interval) does not entail an appreciable lowering of the attainable (uniform) reflection coefficient.

3. Broadband molybdenum-silicon mirrors for dispersion spectroscopy

Calculated at the first stage was an aperiodic MS (40 Mo/Si layer pairs).The thicknesses $\{l_i\}$ of all 80 layers of Mo and Si were treated as independent variables (optimisation parameters). The existence of $MoSi_2$ transition layers, which were formed in the structure synthesis, was also taken into account. Their thicknesses were assumed to be fixed and equal to 12 Å (Mo-on-Si) and 6 Å (Si-on-Mo). The structure of this type ($Si/MoSi_2/Mo/MoSi_2 \ldots Si/MoSi_2/Mo/MoSi_2/Substrate$) was optimised to achieve the highest possible uniform reflectivity throughout the 12.5–25 nm interval at normal radiation incidence. The result of optimisation is shown in Fig. 4: the layer thicknesses of the optimal aperiodic MS (Fig. 4a) and its calculated reflection coefficient in the 12.5–30 nm range

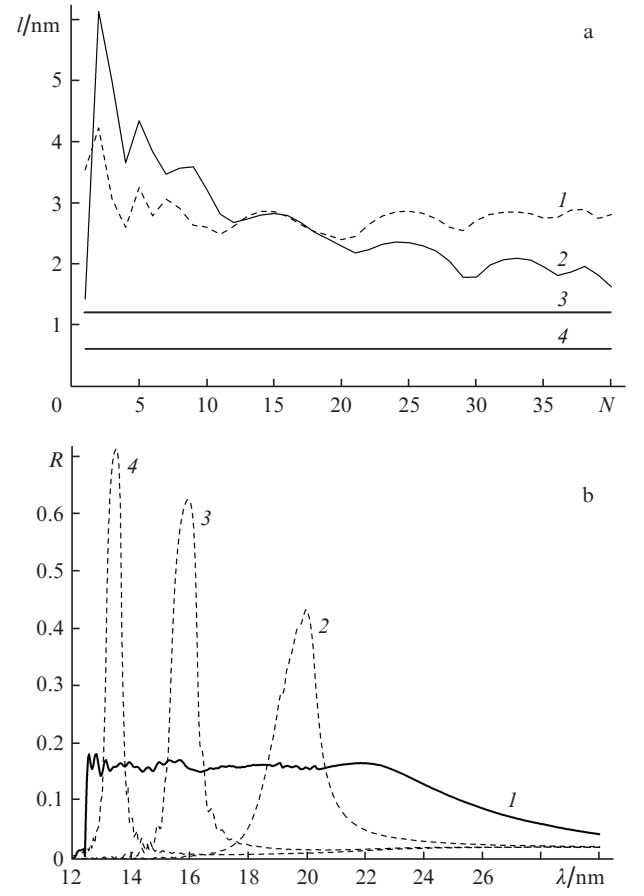

Figure 4. Layer thicknesses of Mo (*1*), Si (*2*), and transition (Mo-on-Si) (*3*) and (Si-on-Mo) (*4*) layers of the aperiodic MS optimised for maximum uniform reflectivity in the 12.5–25 nm interval (the thicknesses of transition layers are fixed, the layer numbering increases downward from top to substrate) (a). Calculated reflection coefficient of this aperiodic MS in the 12–30 nm range at normal radiation incidence (*1*). Shown for comparison are the reflection coefficients of periodic MMs optimised for maximum reflection coefficients at wavelengths of 20 (*2*), 16 (*3*), and 13.5 nm (*4*) (b).

(Fig. 4b). The integral reflectivity of this structure taken over the 12.5 – 25 nm interval is equal to 1.97 nm and to 2.32 nm when taken over the 12.5 – 30 nm interval. In this case, the reflection coefficient averaged over the 12.5 – 25 nm optimisation interval is equal to 15.8%. Without the inclusion of transition layers, the average reflection coefficient of the corresponding optimised AMS is equal to 17.2%, i.e. the relative lowering of the 'plateau' level is equal to 8%.

Next the MSs corresponding to the calculated ones were deposited on concave spherical substrates by argon ion sputtering of targets in vacuum (National Technical University 'Kharkov Polytechnic Institute', KhPI). The synthesised MMs were investigated at the KhPI from the reflection of radiation with a wavelength of 1.54 Å at grazing incidence; at the Institute for Physics of Microstructures (IPM), Russian Academy of Sciences (RAS), their reflectivity was measured at several wavelengths in the operating range (12.5 – 30 nm) at normal radiation incidence; at the P.N. Lebedev Physical Institute (LPI), RAS, the uniformity of reflection was estimated using a broadband laser-plasma source of VUV and SXR radiation. The synthesised MS proved to be sufficiently close to the calculated one and the relative uniformity of the reflection coefficient was equal to ~15% [12–15]. It is noteworthy that the reflection coefficient in the long-wavelength part of the operating range (25 – 30 nm) turned out to be somewhat higher than the calculated one.

These aperiodic MSs deposited on concave fused silica substrates of radius 1 or 0.5 m with a surface roughness of 3–5 Å were repeatedly employed to record space-resolved plasma spectra with the use of spectrographs represented schematically in Fig. 1. Below we cite several examples that demonstrate the virtues of this imaging (stigmatic) spectrograph.

We estimated the spatial, spectral, and temporal characteristics of the debris-free SXR radiation source excited in a pulsed xenon jet in vacuum [16–18]. In the experiment we recorded: the resultant plasma spectrum in the 12.5–25 nm range; quasimonochromatic plasma images formed by the radiation with $\lambda \approx 13.5$ and 18 nm; the absolute intensity of emission at these wavelengths as well as the temporal shape of quasimonochromatic SXR radiation pulses. Figure 5 shows the image of xenon plasma formed by its 13.5-nm radiation, which was recorded using a periodic MM with the reflectivity peak at $\lambda \approx 13.5$ nm in combination with a free-standing multilayer Zr/Si absorption filter. About one hundred spectral lines and unresolved line groups were observed in the xenon spectrum in the 12.5–25 nm range. Figure 6 shows one of Xe spectrograms with indication of several identified lines belonging to the ions Xe VIII–Xe X. The maximum of Xe emission spectrum falls on the 14.5–17 nm region. The decrease in the emission intensity for $\lambda < 14.5$ nm is due to the photoabsorption in the relatively cool periphery of the xenon jet, which surrounds the plasma volume responsible for the SXR emission. This is borne out, in particular, by the fact that the short-wavelength intensity decrease in the spectrum changes under variation of the laser beam axis position relative to the jet axis; changed in this case is the thickness of absorbing layer along the line of sight. This absorption may be so strong that the radiation with wavelengths shorter than 15 nm emanating from the central part of the plasma column is almost completely absorbed, only the emission from the upper and lower parts of the column being observable. The observed 'splitting' begins in the λ ~16–17 nm region and increases with decreasing wavelength to become as large as

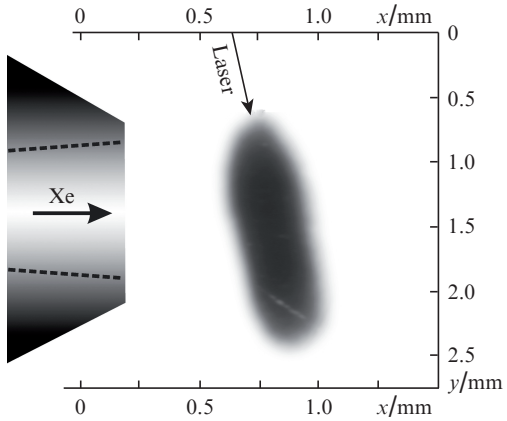

Figure 5. Quasi-monochromatic image of xenon plasma produced by the radiation with a wavelength of 13.5 nm, which was recorded using a periodic MM with a reflectivity peak at $\lambda \approx 13.5$ nm in combination with a free-standing multilayer Zr/Si absorption filter (shown conventionally at the left is the nozzle of gas valve). The emission region has a bell-shaped intensity peak with dimensions (FWHM) of 1.45 mm along the laser beam axis and 0.24 mm in the transverse direction.

1.3 mm – the jet diameter at the base at a distance of 0.5 mm from the nozzle. Shown at the bottom of Fig. 6 is the calculated transmittance of a 0.5-mm thick layer of neutral xenon with a density of 2.2×10^{18} cm^{-3} ($p = 0.09$ atm). One can see that the absorption becomes stronger with decreasing wavelength from 20 to 12.5 nm, where the optical thickness $\tau = \mu_a n_{XeI} r \approx 3$ (μ_a is the photoabsorption cross section, n_{XeI} is the density of XeI atoms, and r is the jet radius). The strong photoabsorption in the range of interest is primarily due to photodetachment of a 4d-electron in neutral Xe I. (The 4d-electron binding energy in neutral xenon is equal to 69.5 eV, which corresponds to a wavelength of 17.8 nm.) Therefore, the stigmatism of the spectrometer enabled demonstrating the role of reabsorption in the formation of the spatio-spectral picture of the emission intensity of the laser-plasma SXR source excited in a Xe jet in a vacuum.

We carried out the spectroscopic investigation of the charge exchange of multiply charged ions of laser plasma with the atoms of a rare-gas jet in a vacuum [19, 20]. The laser plasma was produced by irradiating solid targets with the output pulses of a neodymium-doped yttrium orthoaluminate crystal laser (Nd : $YAlO_3$, 0.5 J, 6 ns, 1.08 μm). The axis of the gas jet was parallel to the plane target and passed at a distance

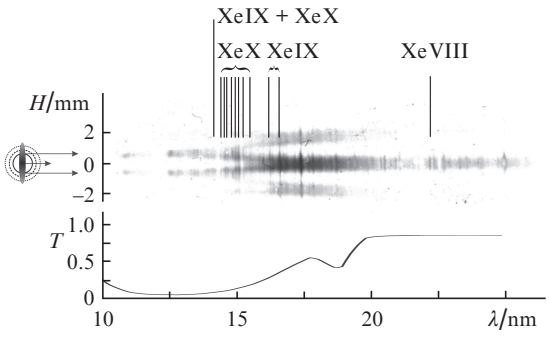

Figure 6. Spectrogram of Xe emission with indication of several identified lines belonging to the ions Xe VIII–Xe X and transmittance of a 0.5-mm-thick Xe layer with a density of 2.2×10^{18} cm^{-3}.

of ~1 cm from it (Fig. 7). The multiply charged ion flux produced by focusing the nanosecond laser pulses on the solid target was directed onto the supersonic jet to give rise to the charge exchange in the interaction with the jet. The field of view of the spectrograph amounted to 20 mm vertically and covered both the region of laser-plasma emission and the charge-exchange region, making it possible to record the spatial picture of the plasma–gas interaction. The distance between the axis of the plasma plume cone and the axis slit was equal to 15 mm; in view of the spectrograph acceptance angle this gives an SXR radiation detection field of width 0.75 mm. The simultaneous recording of a large number of spectral lines in the charge-exchange region enabled acquiring information about the distribution of charge-exchange products over the ion charge states and energy levels.

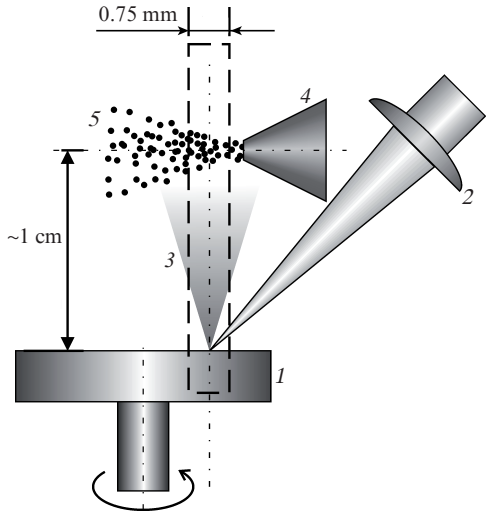

Figure 7. Mutual arrangement of laser-plasma expansion cone and the rare-gas jet: (*1*) rotatable target; (*2*) lens, which focuses laser radiation; (*3*) laser plasma; (*4*) nozzle of a pulsed gas valve; (*5*) gas jet (the dashed lines limit the field of view of the spectrograph).

In the irradiation of a boron target we recorded the charge exchange of B^{5+} nuclei with He, Ne, and Xe atoms (with ground-state ionisation potentials of 24.6, 21.6, and 12.1 eV), which was attended with the population of the excited states of hydrogen-like B V ions with $n = 3$, 4, and 5 (Fig. 8a). The experiment involved the recording of the spectral lines arising from Balmer series transitions H_α ($3 \to 2$, $\lambda = 26.24$ nm), H_β ($4 \to 2$, $\lambda = 19.44$ nm), and H_γ ($5 \to 2$, $\lambda = 17.35$ nm). The partial charge-exchange cross sections were estimated from the relative intensities of the Balmer lines (with the inclusion of cascade radiative transitions) (Fig. 8b). As the ionisation potential of donor atoms lowered, the 'centre of gravity' of charge exchange shifted towards higher n, which reflected the quasiresonance nature of the charge exchange. Also, in Ref. [20] an investigation was made of the multielectron charge exchange of fluorine ions with Ne atoms. For a laser target, in the experiment use was made of a rotatable LiF disc, the lines of Li ions facilitating identification of the spectrum. Figure 9 shows the spatio-spectral picture of the charge exchange recorded in the experiment with a sharp focusing of the laser beam (i.e. with high ion multiplicities in the laser plasma). The vertical axis gives information about the spatial distribution of the radiating

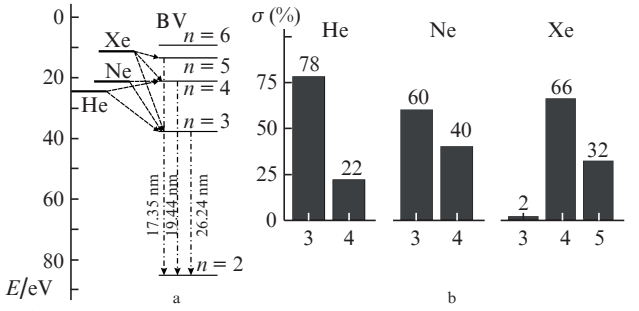

Figure 8. Diagram of the charge exchange of boron nuclei (B VI) with He, Ne, and Xe rare-gas atoms. The dashed arrows show the electron transitions from a donor atom to a B V multiply charged ion, the dash-dotted lines indicate the observable transitions of the Balmer series (a). Variation of the distribution of the partial charge-exchange cross sections over the levels of B V ions with change of gas (b).

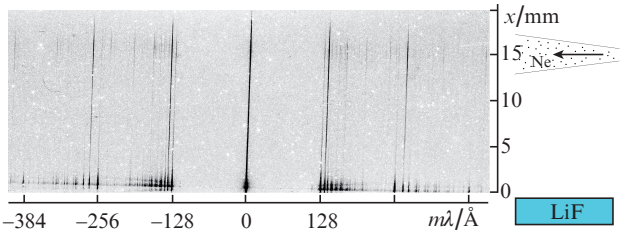

Figure 9. Spatio-spectral picture of the charge exchange of lithium and fluorine ions with neon jet atoms.

ions along the distance from the target surface and the horizontal axis is the dispersion axis. One can see that the emission spectra in the plasma production region and in the charge-exchange region are radically different.

Recently a broadband Mo/Si MM optimised for maximum uniform reflectivity in the 12.5–25 nm range was employed to record the SXR spectra of the radiation reflected from a relativistic 'flying mirror' [22–24]. In this experiment use was made of a slitless version of the SXR spectrograph depicted in Fig. 1. Figure 10 shows the spectrum recorded in the reflection of a femtosecond Ti:sapphire laser pulse from the relativistic plasma wake wave (the flying mirror) driven by the femtosecond pulse of a multiterawatt laser. The visible-to-SXR radiation conversion takes place due to the double Doppler effect. The SXR radiation emanates from the domain of diameter ~16 μm, which approximately corresponds to the focal spot dimension (in a vacuum) of the driving multiterawatt laser radiation.

4. Broadband multilayer mirrors in the region $\lambda \leqslant 12.5$ nm

Advancement below the Si L edge, i.e. to the region of wavelengths shorter than 12.5 nm, calls for the use of material pairs other than Mo/Si. An analysis of the optical constants of elements showed that the best results were to be expected from uranium-containing multilayer structures (naturally, the case in point is depleted uranium, which is composed primarily of ^{238}U). We carried out calculations of different aperiodic MSs in the range 6.7–11.1 nm, which rely on the optical constants of pure materials. Specifically, they show that an aperiodic U/B_4C multilayer structure is capable of affording a uni-

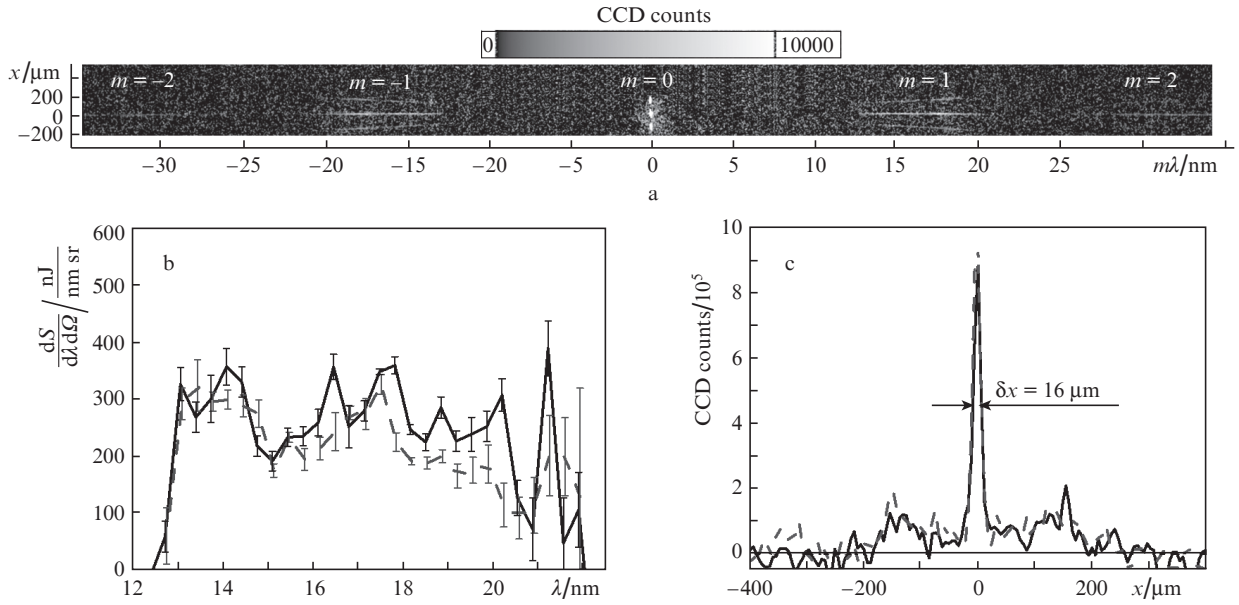

Figure 10. Spectrum of the radiation reflected from a relativistic 'flying mirror' [22–24]; part of the image recorded with an X-ray CCD detector; one can see several orders of diffraction by the grating (5000 lines mm^{-1}) and its support structure (250 lines mm^{-1}, perpendicular to the working lines) (a); emission spectra obtained in the st and –1st diffraction orders (S is the total energy of the SXR pulse) (b). Vertical sections of the spectrum in the 1st and –1st diffraction orders, which characterise the dimension (FWHM) of the SXR radiation source (c).

form reflectivity of ~7.5% throughout the 6.7–11.1 nm interval and a U/C structure a reflectivity of ~4% throughout the 4.4–7 nm interval. Quite good results might be expected from the La/B_4C pair (~4.2%) in the 6.7–11.1 nm region.

Several papers are concerned with the optical properties of uranium-bearing mirrors [32–34]. At the same time, to our knowledge there are no reports in the literature about the synthesis of stable MMs with the nanolayers of chemically pure uranium. This is hindered by the high chemical activity of uranium (it oxidises and becomes friable, unless the uranium film is under ultrahigh vacuum conditions). In the analysis of the problem of fabrication of stable MMs based on uranium-bearing materials, the authors of Ref. [35] arrived at a conclusion that for the $\lambda > 4.5$ nm range it is expedient to make use of uranium carbides (UC, U_2C_3) and may be of a three-component substance of the type $(UC)_{1-x}(UN)_x$. However, it is evident that the advantage of uranium as the bearer of favourable optical constants will wane as the fraction of uranium atoms in the uranium-containing layer is made smaller. The synthesis of periodic La/B_4C(B_9C) MMs for a wavelength of ~ 6.7 nm has been reported [36, 37]. However, their reflectivities at normal incidence turn out to be substantially lower than the theoretical limit, which is attributable to the formation of relatively thick transition layers.

Good results are furnished by beryllium-containing MMs. The synthesis of a periodic Mo/Be mirror (70 periods) with a reflectivity of 68.7% at a wavelength of 11.3 nm has been reported [38]. Calculations suggest that one might expect a normal-incidence reflectivity of ~0.2 throughout a 11.1–13.5 nm band from broadband aperiodic beryllium-containing MMs (23% from Rh/Be and 20% from Mo/Be MMs). Unfortunately, beryllium-containing MMs are efficient only down to the K absorption edge of Be (about 11.1 nm).

This state of affairs has impelled us to resume the quest for material pairs suited for the fabrication of efficient aperiodic MMs for the wavelength region below ~13 nm. We therefore set ourselves the goal of elucidating the possibility, in principle, of fabrication of broadband normal-incidence mirrors in the $\lambda < 13$ nm domain and calculating their highest performance characteristics determined by the optical constants of the corresponding elements. In doing this we operate on the premise that technological problems, should they emerge in the path of synthesis of these mirrors, will be overcome, much like the difficulties encountered in the making of stable Mg/Si MMs, by way of introduction of barrier layers to prevent the interdiffusion of the main layer materials of the structure [39].

Attempts to formulate an analytical criterion indicating the optimal material pair for the solution of the problem in hand do not meet with success. The final judgement is reached proceeding from numerical solutions. However, it is well known that the reflection from each interface becomes stronger with increasing the difference between δ and β of the corresponding substances. That is why there is good reason to select for the MMs the pairs of materials with a high reflectivity at their interface and not-too-high an absorption coefficient, so that the effective number of interfering beams is high enough.

We analysed the optical constants of 18 materials (Y, Zr, Nb, Mo, Ru, Rh, Pd, Ag, Si, B_4C, C, Ti, Co, W, Ni, Cr, Sb, Sc), which are void of absorption edges in the 8–12.5 nm range, and selected the most promising ones for the fabrication of MMs in this domain. The real part of the refractive index of palladium departs significantly from unity in comparison with other elements, while the imaginary constituent is not too large in the domain of interest, which underlies the choice of palladium as the first MM component. Y and B_4C are best suited for the second component. Numerical experiments suggest that Pd/Y and Ag/Y are the best material pairs for the fabrication of MMs in the spectral domain specified above.

Figure 11 shows the calculated reflection coefficients of different periodic MSs optimised for maximum normal-incidence reflectivity at a wavelength of 9 nm (without inclusion

of transition layers and substrate roughness). The best results are to be expected from the pairs Pd/Y (62%), Ag/Y (62%), Rh/Y (60%), and Pd/B_4C (58%). The number of MS levels was selected in such a way as to achieve the effect of saturation. The values of the peak reflection coefficient, the spectral width (FWHM) of reflection peak, and integral reflection coefficient $\Im_\lambda$ taken over the 8–10 nm range are collected in Table 1 for several MSs.

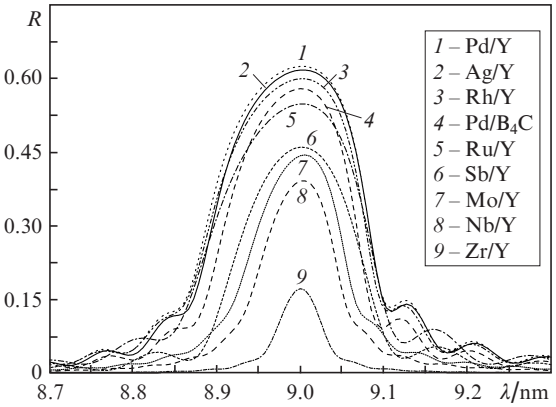

Figure 11. Spectral reflectivity profiles of Pd/Y, Ag/Y, Rh/Y, Pd/B_4C, Ru/Y, Sb/Y, Mo/Y, Nb/Y, and Zr/Y MSs optimised for maximum reflectivity at $\lambda = 9.0$ nm (without inclusion of transition layers).

Table 1. Reflection characteristics of periodic MSs with a reflectivity maximum at a wavelength of 9 nm (calculation without the inclusion of transition layers).

Material pair	N	R_{max} (%)	FWHM/nm	J_λ (nm) over the 8–10 nm region
Pd/Y	200	62	0.192	0.147
Ag/Y	200	62	0.186	0.140
Rh/Y	200	60	0.186	0.138
Pd/B_4C	200	58	0.160	0.114
Ru/Y	150	55	0.191	0.125
Sb/Y	150	46	0.153	0.083
Mo/Y	300	44	0.119	0.069
Nb/Y	350	39	0.099	0.051
Zr/Y	400	17	0.058	0.014

In the calculation of broadband MMs, all layer thicknesses were the optimisation parameters. The long-wavelength bound of optimisation domain was fixed at $\lambda = 13$ nm, while the position of the short-wavelength bound was varied. The Ag/Y and Pd/Y structures optimised for maximum uniform reflectivity in the 9–13 nm range at near-normal incidence (5°) afford respective reflectivities of 11.5% and 11.4%. Shifting the short-wavelength bound to 8.5 nm lowers the attainable uniform reflection coefficients of these structures to 9.5% and 9.2%. In the 8–13 nm range the optimised Ag/Y structure is capable of affording a uniform reflection coefficient of 7.2 %. The Rh/Y structure affords $\bar{R} = 8.0\%$ in the 9–13 nm range, and the Pd/B_4C structure gives $\bar{R} = 8.8\%$ (Fig. 12). The integral reflection coefficient ($\Im_\lambda = \int R(\lambda)d\lambda$) taken over the 7.5–15 nm for the Ag/Y structures optimised for maximum uniform reflectivity in the 9–13, 8.5–13, and 8–13 nm intervals amounts to 0.517, 0.495, and 0.396 nm, respectively. The values of uniform reflection coefficient in the specified optimisation intervals as well as the values of

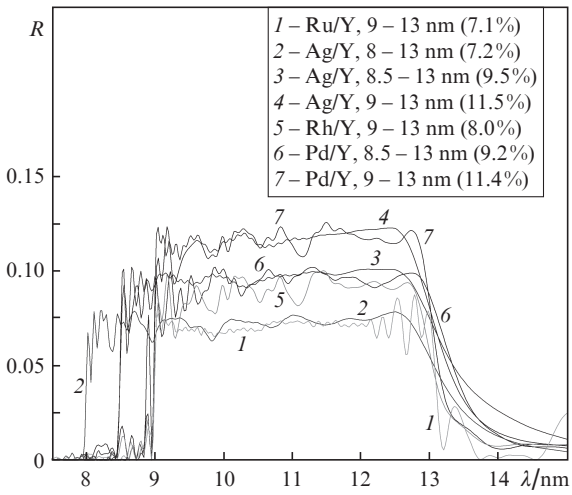

Figure 12. Spectral reflectivity profiles of Pd/Y, Ag/Y, Rh/Y, and Ru/Y MSs optimised for maximum uniform reflectivity in the ranges 8–13, 8.5–13, and 9–13 nm (without the inclusion of transition layers).

Table 2. Reflection characteristics of aperiodic MSs (calculation without the inclusion of transition layers).

Material pair	N	Optimisation range/nm	$\bar{R}$ (%)	J_λ (nm) over the 7.5–15 nm region
Ag/Y	200	9 – 13	11.5	0.517
Ag/Y	200	8.5 – 13	9.5	0.495
Ag/Y	200	8 – 13	7.2	0.396
Pd/Y	150	9 – 13	11.4	0.497
Pd/Y	150	8.5 – 13	9.2	0.470
Rh/Y	200	9 – 13	8.0	0.388
Ru/Y	150	9 – 13	7.1	0.312
Pd/B_4C	150	9 – 13	8.8	0.38

integral reflectivity taken on a wavelength octave of 7.5–15 nm are collected in Table 2 for several structures. As far as we know, the parameters of transition layers in Ag-containing MSs have not been reported.

5. Broadband polarisation elements based on aperiodic structures

As pointed out in Ref. [3], aperiodic MSs can serve as broadband specular polarisers for a fixed angle of radiation incidence. Aperiodic MSs were optimised for maximum uniform reflectivity in the ranges 8.8–12.4 nm (a Rh/B_4C structure, optimal angle of incidence $\theta = 42.5°$), 13–19 nm (Mo/Si, $\theta = 41°$), and 19–30 nm ($MoSi_2$/Si, $\theta = 41.5°$), which were practically nonreflective for p-polarised radiation in these ranges. Specifically, the polarisance $P(\lambda) = (R_s - R_p)/(R_s + R_p)$ of a Mo/Si-based polariser varies from unity to 0.94 throughout its working range and lowers 0.88 for $\lambda = 20$ nm. In this case, the calculated reflectivity for s-polarised radiation is equal to 34% (without the inclusion of transition layers).

More recently, a one-mirror polariser with a spectral width of 3 nm centred at a wavelength of 14.25 nm was synthesised in Ref. [40]; in doing this the authors took into account the formation of transition layers in the form of silicide $MoSi_2$ of fixed thickness (see above). Owing to this the measured reflection coefficient for s-polarised radiation (~0.2) turned out to be close to the calculated one and was sufficiently uniform.

The authors of Ref. [41] reported the fabrication of three broadband polarisers, which were based on aperiodic Mo/Si structures, for the ranges 15–17, 14–18, and 13–19 nm. In all three cases the measured value of $P(\lambda)$ turned out to be close to the calculated one throughout the operating wavelength interval, the measured operating interval-averaged values being equal to 0.987, 0.986, and 0.980, respectively. The reflection coefficients were somewhat lower than the calculated ones and varied in the limits 36%–38%, 17%–25%, and 15%–27% versus calculated average values of 50.05, 35.0%, and 30.4%, respectively. Presumably no account was taken of transition layers in this case.

The authors of Ref. [42] reported the fabrication of broadband Mo/Y polarisers for the regions 8.5–10.1 and 9.1–11.7 nm with reflectivities of 5.5% and 6.1% for s-polarised radiation. In this case, the measured average polarisance was equal to 98.79% ± 0.32% and 96.48 % ± 0.70%, respectively.

A phase-shifting optical element, which was an aperiodic Mo/Si multilayer structure deposited over a silicon nitride membrane, operating at transmission mode was calculated and synthesised in Ref. [43]. The measured phase shift between s- and p-polarised radiation was equal to 42° in the wavelength range 13.8–15.5 nm.

Using material pairs which are optimal for the 9–13 nm range (see Section 4), we calculated a MS possessing the maximum uniform reflectivity in this range for an incidence angle of 42° and simultaneously a high polarisance throughout this range. Plotted in Fig. 13 are the reflection coefficient R_s (the solid curve) and the polarisance P (the dashed curve) of an Ag/Y MS. The average values of R_s and P are equal to 16.9% and 99.4%, respectively.

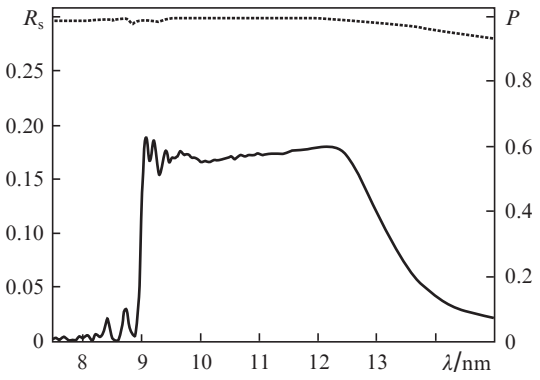

Figure 13. Reflection coefficient (solid curve) and polarisance (dotted curve) of an Ag/Y structure optimised for maximum uniform reflectivity in the 9–13 nm range for an incidence angle of 44°.

6. Conclusions

To date the optics of the SXR spectral range has seen the formation of the research area of aperiodic multilayer optics. The application of multilayer structures broadens the capabilities of multilayer optics and makes it possible to satisfy several optimisation criteria other than attainment of the highest possible reflection coefficient in a relatively narrow range of wavelengths (or incidence angles). Mo/Si multilayer structures possessing uniform reflectivity over a broad spectral range (12.5–25 nm) at normal radiation incidence were synthesised and employed in spectroscopy. In foreign laboratories, keen interest is shown in the synthesis of broadband polarisers operating at a constant incidence angle; a phase shifter operating in transmission mode has also been synthesised. Advancement to the region $\lambda < 12.5$ nm is possible with the use of other material pairs than Mo/Si and may be achieved at the expense of some lowering of uniform reflectivity coefficients. Calculations suggest that it is possible to obtain $\bar{R} = 10\%$ over the 9–13 nm range.

Acknowledgements. This work was supported by the Federal Dedicated Programme 'Scientific and Scientific-Pedagogical Personnel of Innovative Russia' (State Contract Nos 14.740.11.0091 and 02.740.11.0447), the 'Fundamental Optical Spectroscopy and its Applications' Programme of the Physical Sciences Division, RAS, the Regional Public Foundation for the Promotion of National Science, and the Educational-Scientific Complex of the LPI. We take this opportunity to express our appreciation to E.N. Zubarev and V.A. Sevryukova for their help in the execution of electron microscopy investigations.

References

1. Spiller E. *Appl. Phys. Lett*., **20** (9), 365 (1972).
2. Vinogradov A.V., Zel'dovich B.Ya. *Opt. Spektrosk*., **42** (4), 709 (1977).
3. Kolachevskii N.N., Pirozhkov A.S., Ragozin E.N. *Kvantovaya Elektron*., **30** (5), 428 (2000) [*Quantum Electron*., **30** (5) 428 (2000)].
4. Beigman I.L., Pirozhkov A.S., Ragozin E.N. *Pis'ma Zh. Eksp. Teor. Fiz*., **74** (3), 167 (2001) [*JETP Lett*., **74** (3), 149 (2001)].
5. Beigman I.L., Pirozhkov A.S., Ragozin E.N. *J. Opt. A: Pure Appl. Opt*., **4**, 433 (2002).
6. Meekins J.F., Cruddace R.G., Gursky H. *Appl. Opt*., **26** (6), 990 (1987).
7. Van Loevezijn P., Schlatmann R., Verhoeven J., van Tiggelen B.A., Gullikson E.M. *Appl. Opt*., **35** (19), 3614 (1996).
8. Balakireva L.L., Kozhevnikov I.V. *J. X-Ray Sci. Technol.*, **6** (2), 150 (1996).
9. Joensen K.D., Gorenstein P., Wood J., Christensen F.E., Høghøj P. *Proc. SPIE Int. Soc. Opt. Eng*., **2279**, 180 (1994).
10. Ziegler E., Bukreeva I.N., Kozhevnikov I.V., Pirozhkov A.S., Ragozin E.N. *Proc. SPIE Int. Soc. Opt. Eng*., **3737**, 386 (1999).
11. Morawe Ch., Ziegler E., Peffen J.-Ch., Kozhevnikov I.V. *Nucl. Instrum. Methods Phys. Res. A*, **493** (3), 189 (2002).
12. Kondratenko V.V., Levashov V.E., Pershin Yu.P., Pirozhkov A.S., Ragozin E.N. *Kratk. Soobshch. Fiz*., (7), 32 (2001).
13. Ragozin E.N., Kondratenko V.V., Levashov V.E., Pershin Yu.P., Pirozhkov A.S. *Proc. SPIE Int. Soc. Opt. Eng*., **4782**, 176 (2002).
14. Vishnyakov E.A., Mednikov K.N., Pertsov A.A., Ragozin E.N., Reva A.A., Ul'yanov A.S., Shestov S.V. *Kvantovaya Elektron*., **39** (5), 474 (2009) [*Quantum Electron*., **39** (5), 474 (2009)].
15. Ragozin E.N., Mednikov K.N., Pertsov A.A., Pirozhkov A.S., Reva A.A., Shestov S.V., Ul'yanov A.S., Vishnyakov E.A. *Proc. SPIE Int. Soc. Opt. Eng*., **7360**, 73600N (2009).
16. Kapralov V.G., Korde R., Levashov V.E., Pirozhkov A.S., Ragozin E.N. *Kvantovaya Elektron*., **32** (2), 149 (2002) [*Quantum Electron*., **32** (2) 149 (2002)].
17. Levashov V.E., Mednikov K.N., Pirozhkov A.S., Ragozin E.N. *Radiat. Phys. Chem*., **75** (11), 1819 (2006).
18. Levashov V.E., Mednikov K.N., Pirozhkov A.S., Ragozin E.N. *Kvantovaya Elektron*., **36** (6), 549 (2006) [*Quantum Electron*., **36** (6), 549 (2006)].
19. Beigman I.L., Levashov V.E., Mednikov K.N., Pirozhkov A.S., Ragozin E.N., Tolstikhina I.Yu. *Kvantovaya Elektron*., **37** (11), 1060 (2007) [*Quantum Electron*., **37** (11), 1060 (2007)].
20. Beigman I.L., Vishnyakov E.A., Luginin M.S., Ragozin E.N., Tolstikhina I.Yu. *Kvantovaya Elektron*., **40** (6), 545 (2010) [*Quantum Electron*., **40** (6), 545 (2010)].

21. Louis E., Khorsand A.R., Sobierajski R., et al. *Proc. SPIE Int. Soc. Opt. Eng.*, **7361**, 73610I (2009).
22. Kando M., Pirozhkov A.S., Kawase K., et al. *Phys. Rev. Lett*., **103** (23), 235003 (2009).
23. Pirozhkov A.S., Kando M., Esirkepov T.Zh., et al. *AIP Conf. Proc*., **1153**, 274 (2009).
24. Pirozhkov A.S., Kando M., Esirkepov T.Zh., et al. *Proc. SPIE Int. Soc. Opt. Eng.*, **8140**, 81400A (2011).
25. Henke B.L., Gullikson E.M., Davis J.C. *At. Data Nucl. Data Tables*, **54**, 181 (1993); Soufli R., Gullikson E.M. *Proc. SPIE Int. Soc. Opt. Eng.*, **3113**, 222 (1997); <http://henke.lbl.gov/optical_constants/>.
26. Parratt L.G. *Phys. Rev*., **95** (4), 359 (1954).
27. Vinogradov A.V., Kozhevnikov I.V. *Trudy FIAN*, **196**, 62 (1989).
28. Zubarev E.N., Kondratenko V.V., Pol'tseva O.V., Sevryukova V.A., Fedorenko A.I., Yudin S.A. *Metallofizika i Noveishie Tekhnologii*, **19** (8), 56 (1997).
29. Largeron C., Quesnel E., Thibault J. *Phil. Mag*., **86** (19), 2865 (2006).
30. Stearns D.G., Rosen R.S., Vernon S.P. *Proc. SPIE Int. Soc. Opt. Eng.*, **1547**, 2 (1991).
31. Maury H., Jonnard P., André J.-M., Gautier J., Roulliay M., Bridou F., Delmotte F., Ravet M.-F., Jérome A., Holliger P. *Thin Solid Films*, **514**, 278 (2006).
32. Allred D.D., Squires M.B., Turley R.S., Cash W.C., Shipley A.F. *Proc. SPIE Int. Soc. Opt. Eng.*, **4782**, 212 (2002).
33. Sandberg R.L., Allred D.D., Johnson J.E., Turley R.S. *Proc. SPIE Int. Soc. Opt. Eng.*, **5193**, 191 (2004).
34. Artyukov I.A., Vinogradov A.V., Vikhlyaev D.A., Voronov D.L., Kondratenko V.V., Lipin A.V., Ostashev V.I., Pronin V.A., Sagitov S.A., Udovskii A.L., Uspenskii Yu.A., Feshchenko R.M. *Poverkhnost'. Rentgenovskie, Sinkhrotronnye i Neitronnye Issledovaniya*, (5), 9 (2007).
35. Artioukov I.A., Fechtchenko R.M., Udovskii A.L., Uspenskii Yu.A., Vinogradov A.V. *Nucl. Instrum. Methods Phys. Res. A*, **517**, 372 (2004).
36. Platonov Yu.Yu., Gomez L., Broadway D. *Proc. SPIE Int. Soc. Opt. Eng.*, **4782**, 152 (2002).
37. Barysheva M.M., Andreev S.S., Vainer S.A., Gusev S.A., Zuev S.Yu., Pestov A.E., Polkovnikov V.N., Salashchenko N.N., Chkhalo N.N. *Proc. of the Workshop 'X-Ray Optics – 2008'* (Chernogolovka: IPTM RAN, 2008) p. 32.
38. Skulina K.M., Alford C.S., Bionta R.M., Makowiecki D.M., Gullikson E.M., Soufli R., Kortright J.B., Underwood J.H. *Appl. Opt*., **34** (19), 3727 (1995).
39. Zuev S.Yu., Polkovnikov V.N., Salashchenko N.N. *Proc. XII Int. Nanophysics and Nanoelectronics Symp.* (N. Novgorod: IFM RAN, 2008) Vol. 2, p. 227.
40. Aquila A.L., Salmassi F., Dollar F., Liu Y., Gullikson E.M. *Opt. Express*, **14** (21), 10073 (2006).
41. Wang Z., Wang H., Zhu J., Wang F., Gu Z., Chen L., Michette A.G., Powell A.K., Pfauntsch S.J., Schäfers F. *J. Appl. Phys*., **99** (5), 056108 (2006).
42. Wang Z., Wang H., Zhu J., Xu Y., Zhang S., Li C., Wang F., Zhang Z., Wu Y., Cheng X., Chen L., Michette A.G., Powell A.K., Pfauntsch S.J., Schäfers F., Gaupp A., MacDonald M. *Appl. Phys. Lett*., **89** (24), 241120 (2007).
43. Wang Z., Wang H., Zhu J., Zhang Z., Xu Y., Zhang S., Wu W., Wang F., Wang B., Liu L., Chen L., Michette A.G., Powell A.K., Pfauntsch S.J., Schäfers F., Gaupp A., MacDonald M. *Appl. Phys. Lett*., **90** (3), 031901 (2007).